July 5, 2019

Characterizing the local oxidation nanolithography on highly oriented pyrolytic graphite

Zachary H Swart
Alex J Ulrich
Collin D Wick
Adarsh D Radadia

IOP Publishing Nanotechnology
Nanotechnology 30 (2019) 275301 (7pp) https://doi.org/10.1088/1361-6528/ab1181

Characterizing the local oxidation nanolithography on highly oriented pyrolytic graphite

Zachary H Swart[1,4], Alex J Ulrich[1,4], Collin D Wick[3] and Adarsh D Radadia[1,2]

[1] Institute for Micromanufacturing, Louisiana Tech University, Ruston, LA 71272, United States of America
[2] Center for Biomedical Engineering and Rehabilitation Services, Louisiana Tech University, Ruston, LA 71272, United States of America
[3] Chemistry, Louisiana Tech University, Ruston, LA 71272, United States of America

E-mail: radadia@latech.edu

Received 1 February 2019, revised 8 March 2019
Accepted for publication 20 March 2019
Published 16 April 2019

Abstract

Here, we characterize the patterns obtained through local oxidation nanolithography (LON) on highly oriented pyrolytic graphite as the write bias, speed, and force were varied. Different types of patterns—bumps, cracked bumps, and trenches—were obtained and characterized using four shape descriptors—pattern width, pattern height, cut width and cut depth. With an increase in write bias the obtained pattern type varied from bumps to cracked bumps to trenches. The use of a bias above 7.25 V resulted in trenches with increased variability in shape descriptor values. Similarly, an increase in write speed demonstrated a transition from trenches to cracked bumps to bumps. An increase in write force from 75 to 150 nN showed a shift in the threshold voltage from 4.25 V to just under 3.75 V and formed cracked bumps instead of bumps. These findings help solve the mystery of why bumps were not reported at threshold voltages before 2008. We believe these findings will be enable uniform reproduction and report of LON pattern.

Supplementary material for this article is available online

Keywords: AFM, nanolithography, local oxidation, tip-based nanomanufacturing, HOPG

(Some figures may appear in colour only in the online journal)

1. Introduction

Carbon nanomaterials such as graphene [1], carbon nanotubes [2], and fullerenes [3] have drawn significant interest from researchers due to their outstanding physical properties as well as their electrical sensitivity to the environment [4–6]. Along with the conventional photolithography and e-beam lithography, atomic force microscope (AFM) based nanolithography techniques are attractive to build low dimensional devices with carbon nanomaterials as they offer less restrictive conditions for sample environment and require minimum pre- and post-processing. AFM lithography techniques include either mechanically [7], thermally [8], or electrically induced modifications of the sample surface [9, 10]. Local oxidation nanolithography (LON) is an electrically-induced chemical modification of a surface produced on a nanometer scale by a conductive tip brought either in contact or proximity of the sample. Highly oriented pyrolytic graphite (HOPG), due to its relative ease of preparing the atomically flat surface, layered nature and electrical conductivity, has been an ideal substrate for LON patterning. The idea stems from the early experiments in 1989–1992 with a scanning tunneling microscope [11–13]. Researchers have since recognized the role of ambient humidity to form a water meniscus between the tip and the sample. It is hypothesized that the electric field

[4] First authors based on equal contributions.

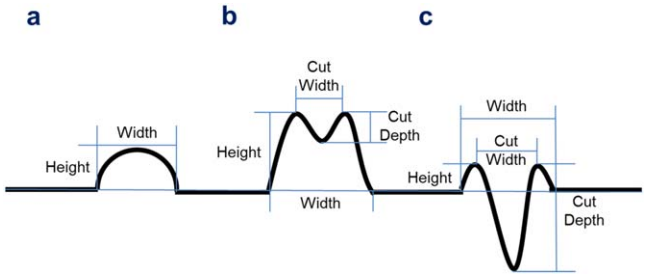

Figure 1. Characteristics recorded for (a) a bump, (b) a cracked bump, and (c) a trench.

between the tip and the sample when above a certain threshold electrolyzes the water into H^+ and OH^- ions, and drives the OH^- ions towards the relatively positive biased sample. The OH^- ions chemically oxidize the sample surface within the range of the meniscus. While scanning tunneling microscopy in air have only reported formation of trenches, studies in water [14], or sulfuric acid solutions [15] have elucidated that formation of bumps precedes the formation of trenches and a threshold tip bias of -4.0 ± 0.2 V is necessary to form bumps.

Similarly, early studies of AFM-assisted LON on HOPG reported the formation of trenches only [16, 17]. Kim and Koo (2003) reported an etch depth less than 4 atoms (almost constant) at a tip bias below −8 V, and in excess of 20 atoms at a tip bias of −10 V. Park *et al* (2007) reported that pulsing the sample bias resulted in formation of 10 nm wide and 0.34 nm deep trench. Jiang and Guo (2008) for the first time demonstrated the formation of bumps (convex structures) on HOPG using AFM-assisted LON [18]. Low sample bias or lithography time was found to form bumps (convex dots), while higher tip bias or lithography time resulted in a trench (concave dots). With a bias duration of 10 s, these bumps were seen to start forming with sample bias in the 2–3 V range, then crack in the 4–5 V range with trenches being prominent above 5 V. In a follow-up study on point patterns, Jiang and Guo (2011) provided a relationship to calculate the threshold time required at any given sample bias to predict the transformation of a bump to a trench [19]. However, the effect of write force was not studied. Further, we find that most lithography masks require patterning lines where the effect of write speed also needs to be accounted. The resultant patterns are much more complicated as shown in figure 1.

In this paper, we study the effect of sample bias, write speed, and write force on the bump-trench transformation and characterize the resultant LON features using shape descriptors (shown in figure 1) that can be used to recreate the pattern more accurately. Past studies have shown the formation of a lip around the trenches but were ignored for characterization purposes. We propose the use of four shape descriptors—overall pattern width, pattern height, cut width, and cut depth—to commonly characterize the LON patterns on HOPG and its variations with a change in sample bias, write speed and write force.

2. Materials and methods

The Arrow EFM probes from Nanoworld were used in this research ($f_0 \sim 75$ kHz, $k \sim 2.8$ N m^{-1}, ~240 μm long, ~35 μm wide and ~3 μm thick, with a 23 nm thick platinum/5% iridium layer deposited on both sides of the cantilever). An Agilent 5420 AFM equipped with a MAC III controller was used to perform local anodic oxidation on ZYB grade HOPG (mosaic spread value: 0.8°; mosaic spread accuracy: ±0.2°; 10 × 10 × 2 mm^3). Picoview version 1.10.1 paired with a PicoLITH package was used for AFM operation. PicoLITH package allowed for the positioning and manipulation along with the capabilities for nanolithography.

The method of reference cantilever array was used to accurately calculated force constant of each Arrow EFM probe [20]. The Sader method was used to calculate the force constant of the reference cantilevers in an All-In-One Tipless probe from Budget Sensors [21]. The reference cantilever thickness, width, and length for the Sader method were obtained via scanning electron microscopy. Out of all the reference cantilevers, the ones with the closest force constant to that expected were used to measure the force constant (k_c) of the Arrow EFM probe as follows

$$k_c = k_r\left[\frac{S_s}{S_r} - 1\right]\cos^2\theta,$$

where k_r was the force constant of the reference cantilever calculated by the Sader method, S_s was the slope of a force curve generated by pressing the Arrow EFM probe against a solid material such as bulk silicon, and S_r was the slope of a force curve generated by pressing at the end of a reference cantilever. The angle (θ) at which the tip was bent during testing was assumed to be 0 for our calculations.

Following, the HOPG was placed under the calibrated AFM probe. A home-made atmosphere control chamber reported earlier [22], was placed enclosing the tip and the sample; the humidity was monitored with an EL-USB-2 + Data Logger. For all lithography, the chamber atmosphere was maintained at ~55% relative humidity for ease and consistency. All lithography was done in contact mode and subsequently scanned in light tapping mode.

To study the effects of the sample on oxidation, a set of lines were patterned varying the bias from 2 to 9.25 V in increments of 0.25 V, while the velocity and force were held constant at 50 nm s^{-1} and 75 ± 5 nN. To study the effect of write speed on oxidation, a set of lines were patterned at 50, 100, 200, 500, 750, and 1000 nm s^{-1}, while holding the force constant at 75 ± 5 nN; the set of lines were written with three different tip bias, 6, 8, and 10 V, in order to record the effect of write speed at different tip bias. In order to study the effect of write force, a write force of 75 ± 5 nN, 150 ± 10 nN, and 225 ± 15 nN the write speed was held constant at 50 nm s^{-1} while varying the voltage from 3.75 to 4.75 V in increments of 0.25 V.

The AFM data was then analyzed using the Gwyddion software package to record the type of pattern (bump, cracked bump, or trench) and its characteristics—pattern width, pattern height, cut width, and cut depth—as shown in figure 1 [23]. Patterns were classified as bumps if the cut depth was less than twice the AFM noise floor. When the cut depth exceeded twice the noise floor, the pattern was classified as a

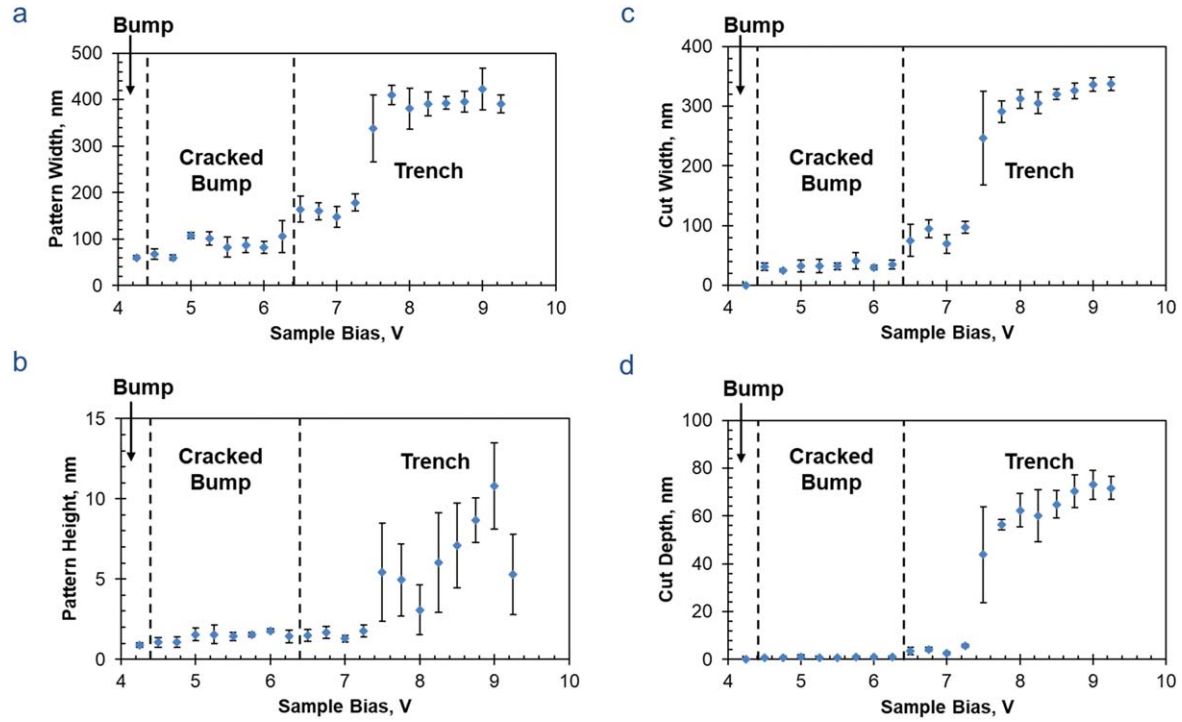

Figure 2. Pattern characteristics as a function of sample bias with a write force of 75 ± 5 nN, a write speed of 50 nm s^{-1}, and ~55%RH: (a) pattern width, (b) pattern height, (c) cut width, and (d) cut depth. Error bars represent standard deviations recorded along the length of a line. Regions are marked on the graph where each type of pattern was observed.

cracked bump if the cut depth was less than the pattern height, else the pattern was defined as a trench.

3. Results and discussion

3.1. Effect of tip bias variation on pattern characteristics

The supporting information figures S1–4 (available online at stacks.iop.org/NANO/30/275301/mmedia) show the topography scans obtained after lithography with a write force of 75 ± 5 nN, a write speed of 50 nm s^{-1}, ~55%RH and varying the sample bias from 3.75 to 9.25 V. The cross-section of the pattern were classified as a bump or a trench, their shape descriptors were calculated (figure 2). Three types of patterns —bumps, cracked bumps, and trenches—were formed, similar to that reported by Jiang and Guo [18]. A threshold voltage of 4.25 V was observed above which the localized oxidation was noticeable in both, the amplitude and the phase images. This is similar to that observed by Jiang and Guo, and also agrees with that reported with STM experiments in air. A sample bias of 4.25 V resulted in a bump, whereas a sample bias between 4.5 and 6.25 V resulted in cracked bumps, and a sample bias above 6.25 V resulted in a trench.

It is expected that the area oxidized will be proportional to the sample bias. Results shown in figure 2 delineate this. A bump that is ~60 nm wide and 0.89 nm high was formed at 4.25 V. At 4.5 V, a cracked bump was formed that was ~68 nm wide and ~1.1 nm high with a ~30 nm wide and ~0.8 nm deep cut. With an increase in sample bias to 6.25 V, the pattern width increased to ~110 nm (~60%) and the pattern height also crept up to ~1.8 nm (~64%), but the cut width and cut depth only increased to ~40 nm (~30%) and ~0.96 nm (~20%), respectively. With an increased sample bias, a larger surface area is expected to oxidize; thus the increase in pattern width is expected. But the correlated increase in pattern height and pattern width can be explained through a plane-wave DFT calculation as shown in figure 3. As the number of oxidized carbon atoms in a graphene plane was increased, its distance from a graphene plane increased by ~6%. But for a cracked bump, a number of graphene planes are expected to oxidize and lead to the overall observed increase of ~60% in pattern height.

As shown in figure 2, the transition from a cracked bump to a trench at 6.5 V was marked by a sudden jump in three shape descriptors—pattern width from ~110 to ~165 nm, cut width from ~35 to ~75 nm, and cut depth from ~0.96 to ~3.5 nm; a change in pattern height was not observed. Within the trench forming regions marked in figures 2(a)–(d), we find a prominent increase in all shape characteristics going from 7.25 to 7.5 V—pattern width from ~180 to ~340 nm, pattern height from ~1.8 to ~5.4 nm, cut width from ~100 to ~250 nm, and cut depth from ~5.6 to ~44 nm. Further increase of sample bias from 7.5 to 9.25 V led to an increase in pattern height, cut width, and cut depth, while the pattern width stayed almost constant. We also noticed a higher variability in the shape characteristics in the 7.5–9.25 V range.

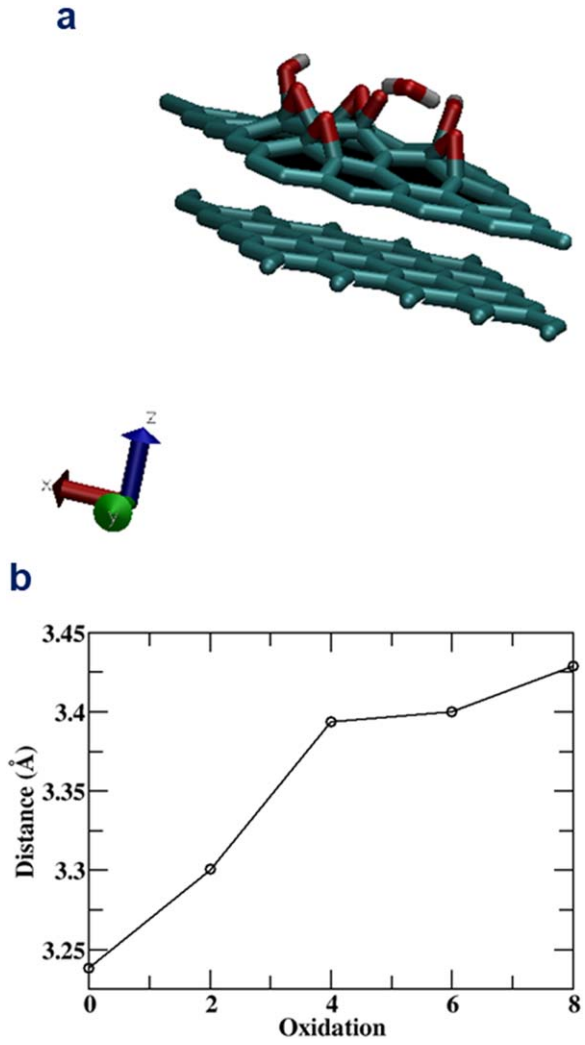

Figure 3. DFT calculation of two graphene planes with 50 atoms in each sheet and cell vectors of 12.33 Å. (a) Molecular scene with one intact graphene plane and second graphene plane with four carbon atoms oxidized. (b) Separation distance, upon geometry and cell optimization, obtained as a function of the number of carbon atoms oxidized in the upper graphene plane. Details of the simulation are provided in the Supporting Information.

3.2. Effect of write speed on pattern characteristics

The supporting information figures S5–7 show the topography scans obtained after lithography with varying write speed between 50 and 1000 nm s^{-1}, a write force of 75 ± 5 nN, 55%RH, and a sample bias of 6, 8, or 10 V. The pattern characteristics obtained are shown in figure 4. It is expected that with the increase in write speed, the tip spends less time per length and thus lower extent of oxidation would occur. We expected trenches with lower write speed; an increase in write speed was expected to form shallower trenches and eventually start forming cracked bumps and then bumps. With a sample bias of 10 V, only trenches were observed and no such transitions. With a decrease in write speed from 1000 to 50 nm s^{-1}, the pattern characteristics were seen to get bigger; pattern width increased from ∼130 to ∼210 nm, cut width from ∼65 to ∼130 nm, cut depth from ∼4 to ∼8.5 nm; only the pattern height stayed between 2 and 3 nm. With a sample bias of 8 V, trenches were observed at a write speed of 50 nm s^{-1} and as the write speed increased a trench to cracked bump transition was noted between 250 and 500 nm s^{-1}. The formation of bumps was not observed. At a sample bias of 6 V, a trench was observed at a low write speed of 50 nm s^{-1} and as the speed was increased a trench to cracked bump transition was noted between 50 and 100 nm s^{-1} and a transition from cracked bump to bump was observed between 250 and 500 nm s^{-1}. With further increase in write speed, eventually formation of no noticeable features was expected, but such threshold write speed was not observed in our experiments.

3.3. Effect of write force on pattern characteristics

The write force controls the tip-sample distance and thus the electric field-gradient between the tip and the sample. It is expected that in cases when bumps or cracked bumps were formed by LON, use of increased write force would lead to the formation of cracked bumps or trenches, respectively. The supporting information figures S8–10 show the topography scans obtained after lithography a write force of 75 ± 5 nN, 150 ± 10 nN, or 225 ± 15 nN, while varying sample bias in an increment of 0.25 V between 3.75 and 4.75 V. A low write speed of 50 nm s^{-1} was used to keep the tip-sample distance nearly constant. The shape descriptors were measured as shown in figure 5. With a write force of 75 ± 5 nN, the bump formation was found to occur at a threshold voltage of 4.25 V. Application of twice the write force (150 ± 10 nN) shifted the threshold voltage just under 3.75 V, and resulted in cracked bumps only. Similar experiment with high write force with the sample bias turned off resulted in no modification of the surface. This confirms that the surface modification at higher write force was due to the sample bias of 3.75 V. Similar surface pattern was also obtained at a write force of 225 ± 15 nN. This shows that the write force can decrease the threshold voltage and change the type of features obtained. For example, work with STM have reported threshold voltage below 4 V. Similarly, this also explains why prior studies on LON with an AFM by Park *et al* [17], and Kim and Koo (2003) [16] never observed bumps; write forces close to ∼500 nN were used. While Jiang and Goo (2008) who first reported bumps, do not mention the write force used, but they do mention the use of a cantilever with a force constant of 1.8 N m^{-1}. We suspect the write force used in their experiment were on the order of 50–100 nN to operate in contact mode.

4. Conclusions

In summary, we delineate the different types of patterns—bumps, cracked bumps, and trenches—formed on HOPG using LON, and propose to characterize these patterns together using four shape descriptors. The role of LON bias, write speed, and write force in determining the pattern type and dimensions have been investigated. The increase in LON bias showed an expected increase in the extent of oxidation. As the

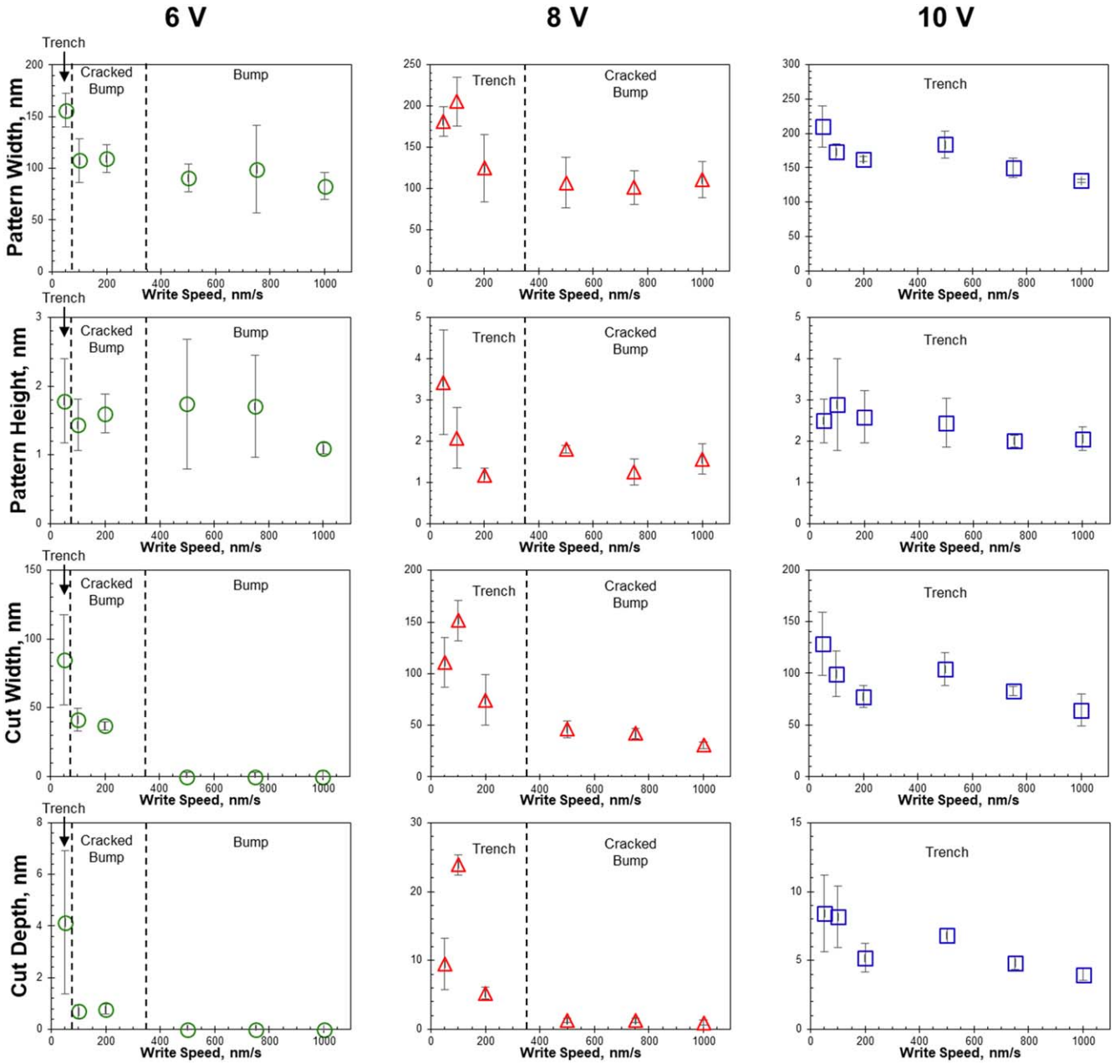

Figure 4. Effect of write speed on pattern characteristics (pattern width, pattern height, cut width, and cut depth). A write force of 75 ± 5 nN and a humidity level of ~55%RH at 22 °C was maintained. The sample bias set at either 6 V (green circles), 8 V (red triangles), or 10 V (blue squares). Error bars represent standard deviations recorded along the length of a line. Regions are marked on the graph where each type of pattern was observed.

LON bias was increased, at low write speed and write force, bumps were observed at 4.25 V, cracked bumps starting 4.5 V, and trenches starting 6.5 V. A region between 7.5 V and above was observed where the shaped descriptors showed a sudden jump in value as well as increased variability. Such a region should be avoided for pattern reproducibility. The increase in write speed showed an expected decrease in the extent of oxidation. With a sample bias of 6 V, a transition from trench formation to the formation of cracked bumps was seen with an increase in write speed, followed by the formation of bumps at high write speeds. With a sample bias of 10 V, only trenches were observed at write speeds as high as 1 μm s^{-1}. The increase in write force from 75 ± 5 nN to 150 ± 10 nN showed a shift in the threshold voltage from 4.25 V to just under 3.75 V. While with higher write forces of 150 ± 10 nN and 210 ± 15 nN the LON patterning could be achieved at a lower threshold voltage, only cracked bumps were observed at these threshold voltages, bumps were only observed with the lower write force of 75 ± 5 nN. These findings help solve the mystery of why bumps were not reported at threshold voltages prior to 2008. Further, we present more detailed guidelines to reproduce the LON features and report a description of the pattern.

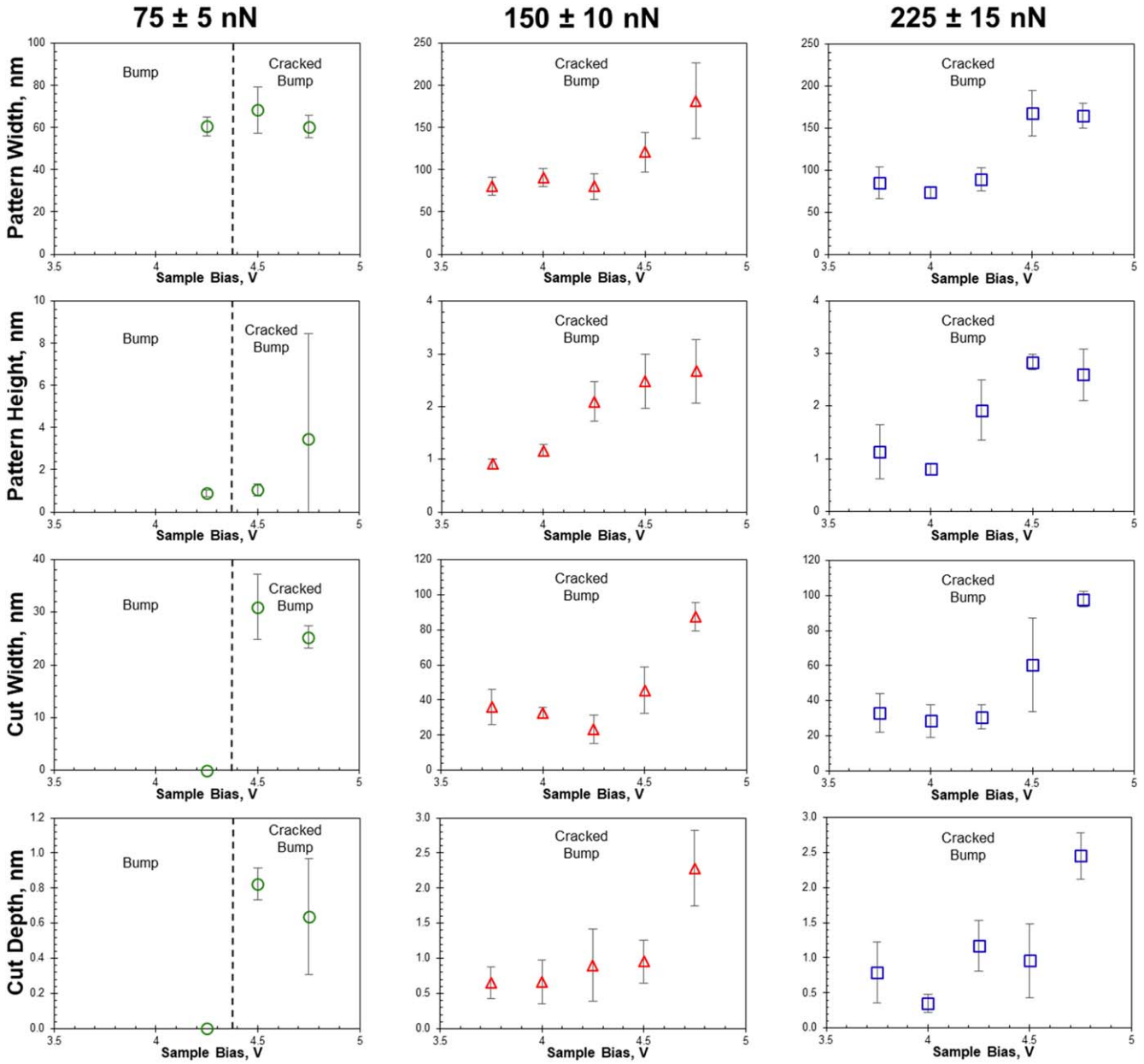

Figure 5. Effect of write force on pattern characteristics (pattern width, pattern height, cut width, and cut depth). The write force was set to either 75 ± 5 nN (green circles), 150 ± 10 nN (red triangles), or 225 ± 15 nN (blue squares). The sample bias was varied between 3.75 V to 4.75 V, with the write speed and the humidity set at 50 nm s^{-1} and ~55%RH at 22 °C, respectively. Error bars represent standard deviations recorded along the length of a line. Regions are marked on the graph where each type of pattern was observed.

Acknowledgments

This material is based upon work partly supported by the Research Competitiveness Subprogram from the Louisiana Board of Regents through the Board of Regents Support Fund under the contract number LEQSF(2013–2016)-RD-A-09; the Research Enhancement Award (subcontract 75537) by the Louisiana Board of Regents Support Fund [LEQSF (2010–2015)-LaSPACE], and the Louisiana Space Consortium through subaward number PO-0000071162 supported by NASA [grant number NNX10AI40H and NNX15AH82H]. We are thankful to A Gunasekaran, D Bailey, and the Agilent AFM technical support for their training and guidance regarding the use and modification of the AFM equipment.

Author contributions

AJU and ADR planned the experiments; AJU conducted the experiments and gathered the data; ZHS and ADR analyzed the data; ZHS and ADR prepared this manuscript.

ORCID iDs

Collin D Wick https://orcid.org/0000-0002-0261-0780
Adarsh D Radadia https://orcid.org/0000-0002-2791-0421

References

[1] Allen M J, Tung V C and Kaner R B 2009 Honeycomb carbon: a review of graphene *Chem. Rev.* **110** 132–45
[2] Endo M, Iijima S and Dresselhaus M S 1997 *Carbon Nanotubes* (Oxford: Pergamon)
[3] Kroto H W, Fisher J E and Cox D E (ed) 1993 *The Fullerenes* (Oxford: Pergamon)
[4] Hasan N, Hou B, Moore A L and Radadia A D 2018 Enhanced ionic sensitivity in solution-gated graphene-hexagonal boron nitride heterostructure field-effect transistors *Adv. Mater. Technol.* **3** 1800133
[5] Hasan N, Zhang W and Radadia A D 2017 Few-flakes reduced graphene oxide sensors for organic vapors with a high signal-to-noise ratio *Nanomaterials* **7** 339
[6] Lee C Y, Sharma R, Radadia A D, Masel R I and Strano M S 2008 On-chip micro gas chromatograph enabled by a noncovalently functionalized single-walled carbon nanotube sensor array *Angew. Chem.* **47** 5018–21
[7] Giesbers A J M, Zeitler U, Neubeck S, Freitag F, Novoselov K S and Maan J C 2008 Nanolithography and manipulation of graphene using an atomic force microscope *Solid State Commun.* **147** 366–9
[8] Wei Z, Wang D, Kim S, Kim S-Y, Hu Y, Yakes M K, Laracuente A R, Dai Z, Marder S R and Berger C 2010 Nanoscale tunable reduction of graphene oxide for graphene electronics *Science* **328** 1373–6
[9] Byun I-S, Yoon D, Choi J S, Hwang I, Lee D H, Lee M J, Kawai T, Son Y-W, Jia Q and Cheong H 2011 Nanoscale lithography on monolayer graphene using hydrogenation and oxidation *ACS Nano* **5** 6417–24
[10] Ekiz O O, Urel M, Guner H, Mizrak A K and Dâna A 2011 Reversible electrical reduction and oxidation of graphene oxide *ACS Nano* **5** 2475–82
[11] McCarley R L, Hendricks S A and Bard A J 1992 Controlled nanofabrication of highly oriented pyrolytic graphite with the scanning tunneling microscope *J. Phys. Chem.* **96** 10089–92
[12] Albrecht T, Dovek M, Kirk M, Lang C, Quate C and Smith D 1989 Nanometer-scale hole formation on graphite using a scanning tunneling microscope *App. Phys. Lett.* **55** 1727–9
[13] Mizutani W, Inukai J and Ono M 1990 Making a monolayer hole in a graphite surface by means of a scanning tunneling microscope *Japan. J. Appl. Phys.* **29** L815
[14] Penner R M, Heben M J, Lewis N S and Quate C F 1991 Mechanistic investigations of nanometer-scale lithography at liquid-covered graphite surfaces *App. Phys. Lett.* **58** 1389–91
[15] Gewirth A A and Bard A J 1988 *In situ* scanning tunneling microscopy of the anodic oxidation of highly oriented pyrolytic graphite surfaces *J. Phys. Chem.* **92** 5563–6
[16] Kim D-H, Koo J-Y and Kim J-J 2003 Cutting of multiwalled carbon nanotubes by a negative voltage tip of an atomic force microscope: a possible mechanism *Phys. Rev.* B **68** 113406
[17] Park J G, Zhang C, Liang R and Wang B 2007 Nano-machining of highly oriented pyrolytic graphite using conductive atomic force microscope tips and carbon nanotubes *Nanotechnology* **18** 405306
[18] Jiang Y and Guo W 2008 Convex and concave nanodots and lines induced on HOPG surfaces by AFM voltages in ambient air *Nanotechnology* **19** 345302
[19] Jiang Y and Guo W 2011 Convex–concave nanostructure transition on highly oriented pyrolitic graphite surface induced by atomic force microscope tip under bias voltage *J. Exp. Nanosci.* **6** 96–101
[20] Gates R S and Reitsma M G 2007 Precise atomic force microscope cantilever spring constant calibration using a reference cantilever array *Rev. Sci. Instrum.* **78** 086101
[21] Sader J E, Chon J W and Mulvaney P 1999 Calibration of rectangular atomic force microscope cantilevers *Rev. Sci. Instrum.* **70** 3967–9
[22] Ulrich A J and Radadia A D 2015 Conductive polycrystalline diamond probes for local anodic oxidation lithography *Nanotechnology* **26** 465201
[23] Nečas D and Klapetek P 2012 Gwyddion: an open-source software for SPM data analysis *Open Phys.* **10** 181–8